Liquid Crystals
Publication details, including instructions for authors and subscription information:
http://www.informaworld.com/smpp/title~content=t713926090

Dielectric properties of selected laterally fluoro-substituted 4,4''-dialkyl, dialkoxy and alkyl-alkoxy [1:1';4':1'']terphenyls

S. Urban[a]; P. Kula[b]; A. Spadło[b]; M. Geppi[c]; A. Marini[c]
[a] Jagiellonian University, Institute of Physics, Krakow, Poland [b] Military University of Technology, Institute of Chemistry, Warsaw, Poland [c] Department of Chemistry and Industrial Chemistry, University of Pisa, Pisa, Italy

Online publication date: 20 October 2010

To cite this Article Urban, S. , Kula, P. , Spadło, A. , Geppi, M. and Marini, A.(2010) 'Dielectric properties of selected laterally fluoro-substituted 4,4''-dialkyl, dialkoxy and alkyl-alkoxy [1:1';4':1'']terphenyls', Liquid Crystals, 37: 10, 1321 — 1330
To link to this Article: DOI: 10.1080/02678292.2010.505665
URL: http://dx.doi.org/10.1080/02678292.2010.505665

Liquid Crystals,
Vol. 37, No. 10, October 2010, 1321–1330

Taylor & Francis
Taylor & Francis Group

Dielectric properties of selected laterally fluoro-substituted 4,4″-dialkyl, dialkoxy and alkyl-alkoxy [1:1′;4′:1″]terphenyls

S. Urban[a], P. Kula[b]*, A. Spadło[b], M. Geppi and A. Marini[c]

[a]*Institute of Physics, Jagiellonian University, Krakow, Poland;* [b]*Institute of Chemistry, Military University of Technology, Warsaw, Poland;* [c]*Department of Chemistry and Industrial Chemistry, University of Pisa, Pisa, Italy*

(*Received 15 March 2010; final version received 10 June 2010*)

Measurements of the complex permittivity, $\varepsilon^* = \varepsilon' - i\varepsilon''$, within the frequency range 200 Hz to 10 MHz for 15 laterally fluoro-substituted terphenyls have been conducted. In most cases the substances exhibited the nematic phase over a broad temperature range. All substances were characterised by negative dielectric anisotropy, and are potentially useful for vertical alignment mode systems. The static permittivity tensor components have been analysed in relation to the dipole structure of the molecules. Dielectric relaxation processes observed in the liquid crystalline (LC) and solid rotator (R) phases (obtained by slow cooling of the samples) are characterised by calculation of the relaxation times and activation barriers. The rotation motions around the short axes are typical for LC phases, whereas rotations about the long axes, accompanied in some cases by internal motions, are present in the R phase.

Keywords: liquid crystal; nematic; negative dielectric anisotropy; dielectric properties; terphenyl

1. Introduction

Liquid crystalline (LC) compounds are a key feature of many electro-optical devices. Their performance depends on the LC material itself, in addition to the state of manufacture of the device. The type of electro-optical effect given by a device requires particular physical properties of the LC materials. Compounds with moderate or large negative dielectric anisotropy ($\Delta\varepsilon = \varepsilon_{\parallel} - \varepsilon_{\perp} < 0$) are attractive for vertical alignment mode (VA) systems, in which the average molecular orientation of the LC material in the off-state is almost perpendicular to the substrate of the display cell. In addition to negative dielectric anisotropy, other important properties of LC materials for displays working in the VA mode include a broad temperature range of the nematic (N) phase, low viscosity, medium birefringence, low rotational viscosity, high thermostability, and photostability. Electro-optical devices operating in the VA mode exhibit very good contrast and high-speed switching. The birefringence and viscosity of LC materials especially affect the switching speed of the display [1–4]. Medium or high birefringence enables the cell gap to be reduced, and a low viscosity is invariably required. Such materials are currently the preferred option for devices such as large flat TV displays and high performance projection micro-displays.

Cells operating in the VA mode exhibit very good contrast and high speed switching [1]. Materials with such properties can be achieved by lateral substitution of polar groups into a mesogenic molecule. An important role is played by fluorine atoms, whose small dimensions and high polarity allow the required properties to be obtained without disrupting the LC nature of the material. Groups of compounds based on a multifluoro-substituted terphenyl core and exhibiting negative dielectric anisotropy, low viscosity and with a nematic phase over a broad temperature range have recently been synthesised [5]. Some of these had previously been synthesised by Merck and also by the group led by Professor G. Gray. The aim of the present paper is to provide an insight into the structure–property relationships of these compounds, characterising their dielectric properties in relation to the positions of the laterally attached fluorine atoms and the types and length of the terminal chains, and how the properties of these materials may be modified as a function of their chemical structure.

2. Experimental

The multifluoro-substituted terphenyls studied are listed in Table 1. Their synthesis and mesomorphic and physical properties have been described by Kula *et al.* [5]. Dielectric measurements were performed using an Agilent 4192A impedance analyser. The thickness of the samples was 0.7 mm, which made the wall orientation effect negligible. The capacitor was filled using a capillary technique. In advance of each measurement it was calibrated using four non-polar substances (*n*-pentane, *n*-hexane, cyclohexane and carbon tetrachloride). In the nematic phase the parallel and perpendicular alignment of the samples was determined

*Corresponding author. Email: pkula@wat.edu.pl

ISSN 0267-8292 print/ISSN 1366-5855 online

DOI: 10.1080/02678292.2010.505665
http://www.informaworld.com

Table 1. Chemical structures and transition temperatures (during heating cycle, in °C) for the compounds studied.

Acronym	Chemical structure	Phase transitions (°C)
KS 1	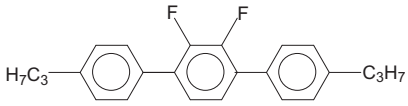	Cr 94 N 130 Iso
KS 2	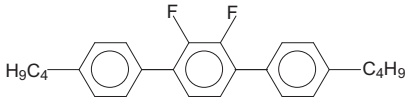	Cr 67 N 102 Iso
KS 3	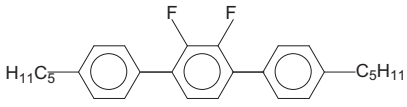	Cr 57.5 N 119.1 Iso
KS 4	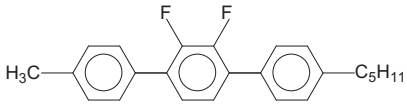	Cr 75.2 N 130 Iso
KS 5	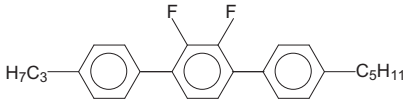	Cr 54.6 N 123.1 Iso
KS 6	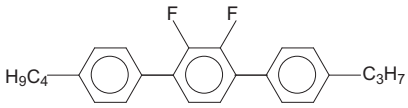	Cr 66.3 N 114.7 Iso
KS 7	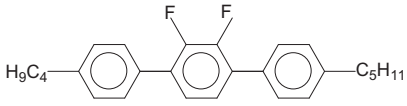	Cr 50.8 N 111.6 Iso
KS 8	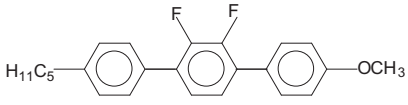	Cr 88.3 N 159.6 Iso
KS 9	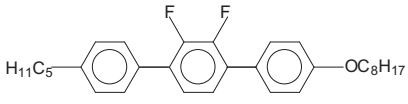	Cr 47.7 S_C 96.3 N 142.2 Iso
KS 10	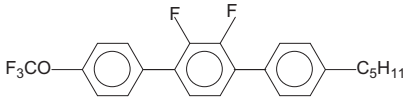	Cr 83.3 (S_B 87.0) S_A 138.6 Iso
KS 11	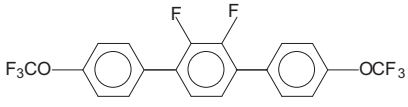	Cr 84.7 N 87.0 Iso
KS 12	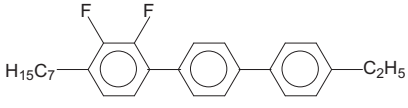	Cr 66.2 S_C 78.7 N 126 Iso

(*Continued*)

Table 1. (*Continued.*)

Acronym	Chemical structure	Phase transitions (°C)
KS 13	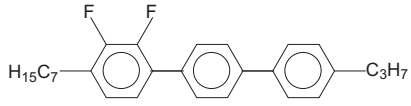	Cr 86.6 S_C 96.4 S_A 119.4 N 138 Iso
KS 14	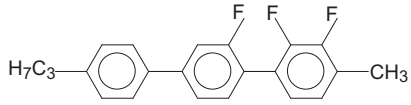	Cr 79.1 N 83.7 Iso
KS 15	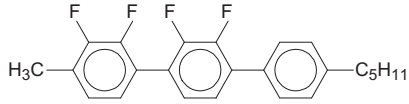	Cr 71.8 (N 69.6) Iso

Note: ( ) denotes monotropic phase.

in a magnetic field of 0.8 T, and saturation of the capacity values *vs.* field was readily achieved. In the smectic phases the samples were not effectively oriented by the magnetic field. The temperature was stable to within ± 0.2 K. All measurements were carried out only during the cooling runs. The complex dielectric permittivity, $\varepsilon^*(\omega) = \varepsilon'(\omega) - i\varepsilon''(\omega)$, was measured in the frequency range 200 Hz–10 MHz. The static value, ε_s, corresponds to the plateau in the low frequency area of the spectra.

A meaningful discussion of the dielectric behaviour in LC phases requires the knowledge of the electric dipole moment structure of the molecules. To achieve this, quantum mechanical calculations were performed using the Gaussian 03 package [6], building all the molecular models using GaussView 5.0. The dipole moments were calculated *in vacuo* at the density functional theory (DFT) level on the optimised molecular structures, using the combination of B3LYP [7, 8] functional with the 6–311g(d) basis set, which offers an acceptable compromise between accuracy and computational cost. The results of calculations for selected compounds are collected in Table 2 and, as an example, Figure 1 shows the configuration of the **KS 1** molecule, the reference frame and the position of the dipole moment, μ.

3. Results and discussion

The dipole structures of the molecules studied (Table 2) clearly indicate that for most of these compounds the dipole moment is substantially aligned with the transverse axis, *x*. This must therefore dominate their

Table 2. Dipole moment (Debye) components and modulus obtained for the compounds investigated, by *in vacuo* DFT [B3LYP/6–311g(d)] calculations.

Compound	μ_x (D)	μ_y (D)	μ_z (D)	μ (D)
KS 1	–2.447	0.002	0.000	2.447
KS 3	–2.494	0.002	0.000	2.494
KS 5	–2.470	0.036	–0.056	2.471
KS 7	–2.511	0.001	0.000	2.511
KS 8	–1.481	0.603	0.543	1.689
KS 10	–2.548	–0.508	–3.091	4.038
KS 12	–2.350	–0.175	0.117	2.359
KS 14	–3.034	–0.176	1.079	3.225
KS 15	–4.006	–0.168	0.009	4.010

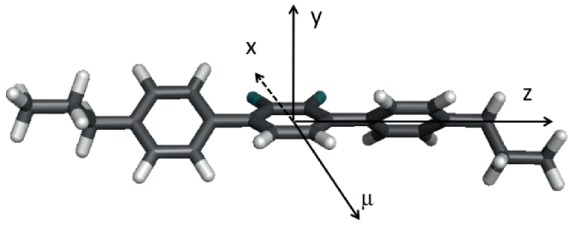

Figure 1. Reference axes for the calculations of dipole moment reported in Table 2, and location of the dipole moment vector (μ) for the compound, **KS 1**.

dielectric properties. The longitudinal μ_l component was close to zero in **KS 1**–**KS 3**, and **KS 11**, due to the presence of molecular symmetry, or very small in the case of **KS 4**–**KS 7**, because the polarity caused by different *n*-alkyl-phenyl components is only slightly dependent on *n* [9]. However, in the case of compounds having non-alkyl lateral substituents (**KS 8**–**KS 10**) or polar cores (**KS 12**–**KS 15**) one might expect a contribution from the longitudinal μ_l dipole component to the relaxation process in the parallel aligned nematic phase. The DFT calculations show a variety of behaviour, ranging from those with a negligible longitudinal dipole moment component (**KS 15**), to those such as **KS 10**, in which the longitudinal component is even slightly larger than the transverse component. The effect described is connected with the molecular rotation around the short axes (flip–flop motion). In the LC phases the relaxation process connected with the molecular rotation around the long axes (spinning motion) usually falls in frequencies in the hundreds of MHz, or even GHz, as is typically observed in dielectric relaxation [10–13] and NMR [14] studies, and is thus beyond the range accessible within the present study.

Analysis of the results was carried out in regard to the structures of the compounds. Compounds in the first group (**KS 1**, **KS 2** and **KS 3**) have the same symmetrical fluoro-terphenyl core and similar terminal alkyl groups on each side of the molecule. The compounds in the second group (**KS 4**, **KS 5**, **KS 6** and **KS 7**) differ from those in the first group in having dissimilar alkyl groups on both sides of the aromatic core, and in the third group (**KS 8**, **KS 9**, **KS 10** and **KS 11**) at least one terminal chain is non-alkyl. In the fourth group (**KS 12**, **KS 13**, **KS 14** and **KS 15**) the aromatic core is no longer symmetrical and also has fluorine atoms on the lateral phenyl moieties, and the aliphatic chains are different on the two sides. Figures 2–5 present (a) the static permittivity components and (b) the dielectric anisotropy for the four groups of compounds. In the nematic phase of all the compounds a negative dielectric anisotropy ($\Delta\varepsilon < 0$) was observed.

3.1 *Static properties*

The static dielectric properties of chemical compounds can be analysed using the Onsager equation (1) [15] for the isotropic phase, and the Maier and Meier equations (2)–(4) [16] for the nematic phase:

$$\frac{(\varepsilon_s - \varepsilon_\infty)(2\varepsilon_s + \varepsilon_\infty)}{\varepsilon_s(\varepsilon_\infty + 2)^2} = \frac{N_0}{3\varepsilon_0}\frac{\mu^2}{3kT} \qquad (1)$$

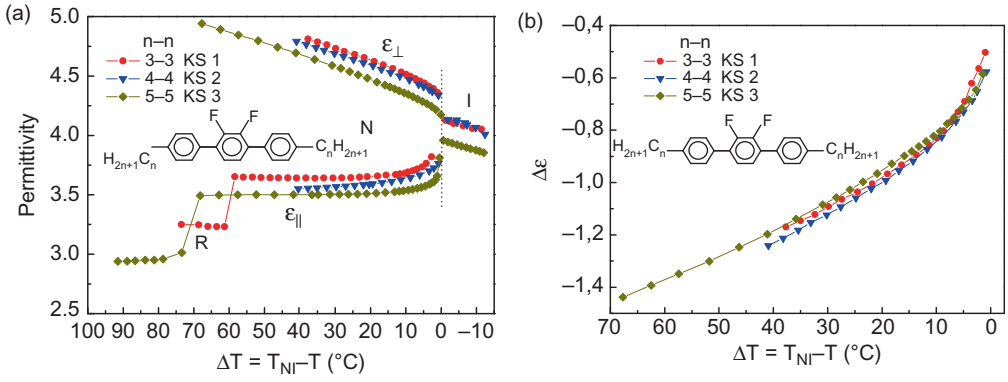

Figure 2. (a) Static permittivity components and (b) dielectric anisotropy for three compounds (**KS 1**–**KS 3**) having the same core and equal alkyl chains lengths, as a function of shift in temperature (colour version online).

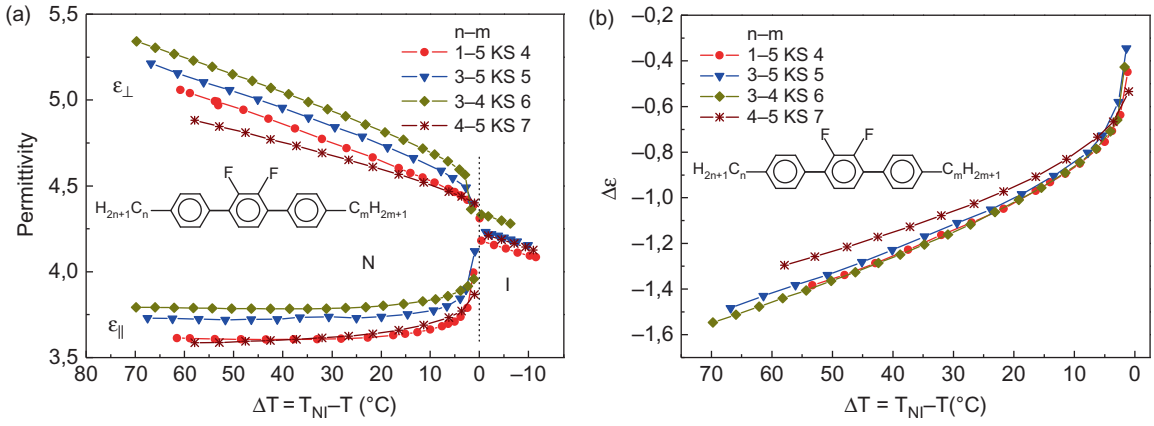

Figure 3. Static permittivity components (a) and dielectric anisotropy (b) for four compounds (**KS 4**–**KS 7**) having the same core and different alkyl chains lengths, as a function of shift in temperature (colour version online).

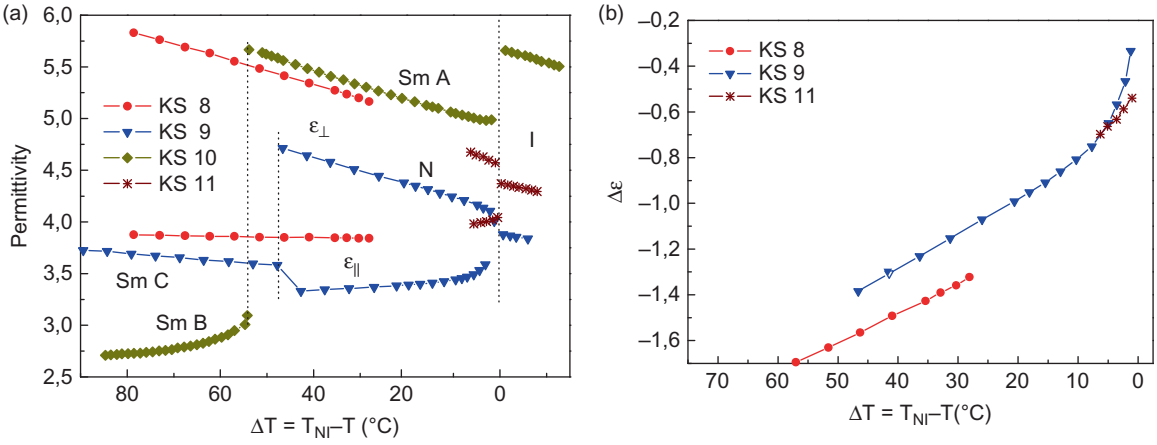

Figure 4. (a) Static permittivity components and (b) dielectric anisotropy for compounds **KS 8**–**KS 11**, which have the same core and different lateral substituents, as a function of shift in temperature. In the case of **KS 10** the sample in the smectic phases could not be aligned (colour version online).

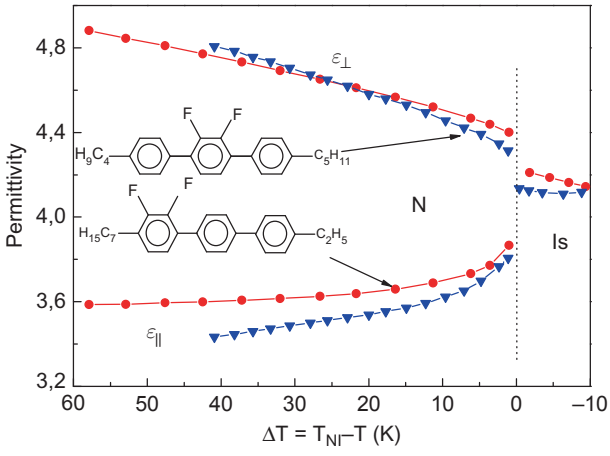

Figure 5. Static permittivity components of two compounds, **KS 7** (circles) and **KS 12** (triangles), having different locations of the fluoro-benzene ring within the molecular core (colour version online).

$$(\varepsilon_{//} - 1) = \varepsilon_0^{-1} N \cdot F \cdot h \cdot \{\bar{\alpha} + \frac{2}{3}\Delta\alpha S + F\frac{\mu_{\text{eff}}^2}{3kT}[1 - (1 - 3\cos^2\beta)S]\} \quad (2)$$

$$(\varepsilon_{\perp} - 1) = \varepsilon_0^{-1} N \cdot F \cdot h\{\bar{\alpha} - \frac{1}{3}\Delta\alpha S + F\frac{\mu_{\text{eff}}^2}{3kT}[1 + \frac{1}{2}(1 - 3\cos^2\beta)S]\} \quad (3)$$

$$\Delta\varepsilon = (\varepsilon_{//} - \varepsilon_{\perp}) = \varepsilon_0^{-1} N \cdot F \cdot h \cdot [\Delta\alpha - F\frac{\mu_{\text{eff}}^2}{2kT}(1 - 3\cos^2\beta)]S, \quad (4)$$

where $N = N_A\rho/M$ (N_A is Avogadro's number, ρ is density and M is molar mass), ε_0 is the permittivity of free space, $\Delta\alpha = \alpha_l - \alpha_t$ and $\bar{\alpha} = (\alpha_l + 2\alpha_t)/3$ are the

anisotropy and the mean value of polarisability, respectively, S is the nematic order parameter, and β is the angle between the total dipole moment, μ, of the molecule and its long axis. The local field factors, F and h, are expressed by the mean permittivity, $\bar{\varepsilon} = (\varepsilon_{||} + 2\varepsilon_{\perp})/3$ [12]. $\mu^2_{\text{eff}} = g\mu^2$ is the square of the effective dipole moment, and g is the dipole–dipole correlation factor. The order parameter $S(T)$ can be determined from the analysis of the experimental anisotropy data with the aid of Equation (4), and then compared with the other results (optical anisotropy and NMR) [17–19]. This will be illustrated in a separate paper.

As it can be seen in Figure 2, the permittivity values for samples of the first group varied slightly with alkyl chain length, but their dielectric anisotropy was virtually similar. It is interesting that in the case of odd numbers of carbons in the alkyl chains (**KS 1** and **KS 3**) the N phase transformed to a rotator (R) phase, exhibiting a pronounced relaxation process, as discussed in the next section of the present paper. The total length of both alkyl tails also had a slight influence on the permittivity values in the second group of substances. For longer tails the permittivity values were reduced (see Figure 3).

The presence of an alkoxy chain in place of an alkyl chain led to an increase in permittivity in the isotropic phase and in the perpendicular component in the N phase (see Figure 4). The methoxy group is the most effective in this respect (**KS 8**).

It is interesting to compare the dielectric properties of compounds having different positions of the difluoro-phenyl ring in the molecular core, for example **KS 7** (in which it is central) and **KS 12** (where it is lateral), but which have the same total chain length (see Figure 5). As might be expected, the parallel component changes noticeably, while the perpendicular component persists unchanged. However, the position of the fluoro-phenyl group influences the phase diagram of these compounds (see Table 1 and Figure 6(a)). One or two fluorine atoms additionally attached to the aromatic core led to a considerable increase in the permittivity value (see Figure 6).

According to Equations (1)–(3), one can assume a rough relationship, $\varepsilon \sim \mu^2$, between the static permittivity and the dipole moment. Taking into account the data in Table 2, the ratios of the transverse components of the square of the dipole moment can be calculated: μ_t^2(**KS 15**)/μ_t^2(**KS 14**) = 1.74, and μ_t^2(**KS 14**)/μ_t^2(**KS 12**) = 1.67. These figures can be related to the respective ratios of the static permittivities of both pairs of substances: 10.40/7.20 = 1.44 and 7.20/4.56 = 1.58 for the perpendicular components in the N phase at the same relative temperature, $T_{NI} - T$, and 8.46/6.22 = 1.36 and 6.22/4.12 = 1.51 for the isotropic phase close to the clearing point. The two sets of experimental ratios (calculated from $\varepsilon_{\perp}$ and ε_{Is} data) were close, but smaller than the respective μ_t^2 ratios. This effect may partly be caused by the antiparallel dipole–dipole correlations with factor $g < 0$. In contrast to this, the pronounced jump in the permittivity value observed at the nematic (N) – rotational (R) phase transition in **KS 14** (Figure 6(a)) clearly indicates the appearance of strong parallel dipole–dipole correlations in the R phase ($g < 0$).

3.2 *Molecular dynamics*

For compounds having the same substituents in both lateral positions, the relaxation process connected with the molecular rotations around the short axes (the flip–flop motion) should not be visible in the spectra measured for parallel-oriented nematic samples ($\mu_z \approx \mu_l \approx 0$). This was the case with **KS 2** and **KS 11**. Unexpectedly, in

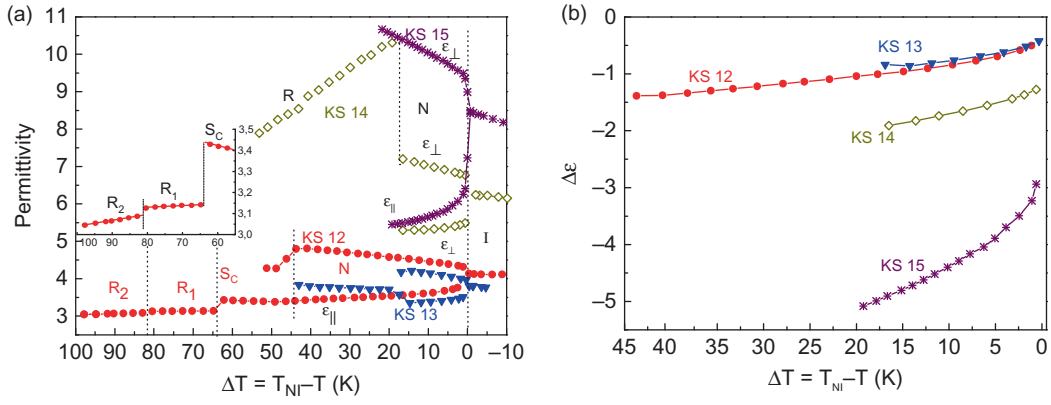

Figure 6. (a) Static permittivity components and (b) dielectric anisotropy for four compounds (**KS 12**–**KS 15**) having different cores and alkyl tails, as a function of shift in temperature (colour version online).

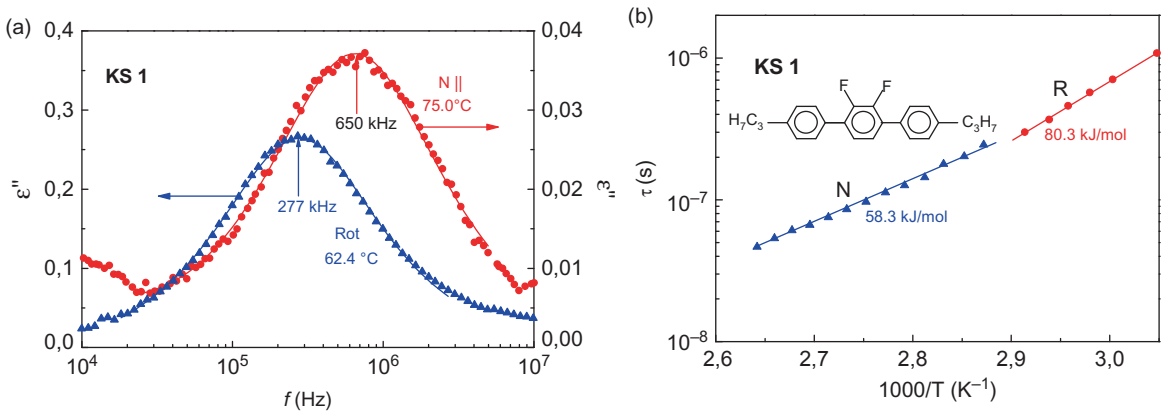

Figure 7. (a) Absorption spectra *vs.* frequency measured for **KS 1** in the nematic phase (dots, parallel orientation, right-hand scale) and in the rotator phase (triangles, left-hand scale). The lines are fits of the imaginary part of Cole–Cole Equation (5). The distribution parameter $\alpha \approx 0$. (b) Dielectric relaxation times *vs.* inverted temperature for the nematic and rotator phases of **KS 1**. The straight lines are plots of the Arrhenius equation $\tau = \tau_0 \exp(\Delta H/RT)$, yielding the activation enthalpies, ΔH, indicated (colour version online).

two compounds, **KS 1** and **KS 3**, which possess odd numbers of carbon atoms in the alkyl tails, the relaxation process was detectable in MHz frequencies, although its amplitude was very small. Figure 7(a) presents the absorption spectrum $\varepsilon''_{\parallel}(f)$ in the nematic phase, which is comparable with that collected in a monotropic rotator phase appearing under a slow rate of cooling. As it can be seen in Figure 2(a), the ε_s value for **KS 1** was markedly diminished at the transition from the nematic to the rotator phase. At the same time the dielectric loss $\varepsilon''(f)$ increased by one order of magnitude (Figure 7(a)). It is certain that both of these relaxation processes originate from different molecular rotations: the flip–flop motion in the nematic phase (in which a very small μ_l component is involved) and the spinning motions in the rotator phase (where a large μ_t component is involved). A similar behaviour was observed for the second compound, **KS 3**, which has an odd number of carbon atoms in the alkyl tails. This indicates that in the nematic phase the long molecular axes are considerably inclined from the *p*-axis of the phenyl rings due to kinks in the alkyl tails, which lead to the creation of a small longitudinal dipole component. However, this was not observed in the DFT calculations for these compounds.

The dielectric relaxation spectra were analysed with the aid of the Cole–Cole function, enriched by the conductivity component,

$$\varepsilon^* = \varepsilon' - i\varepsilon = \sum_k \frac{\varepsilon_{sk} - \varepsilon_{\infty k}}{1 + (i\omega\tau_k)^{1-\alpha_k}} + i\frac{\sigma_0}{\varepsilon_o f}, \qquad (5)$$

where ε_s and ε_∞ are the static and high frequency permittivities, respectively; $\omega = 2\pi f$, in which f is the frequency, τ is the relaxation time, α is a parameter characterising the distribution of relaxation times; σ_0 is the conductivity; and ε_o is the permittivity of free space. k indicates the number of relaxation processes. The dielectric increment, $\varepsilon_s - \varepsilon_\infty$, is proportional to μ^2. In the representation of ε'' *vs.* ε', this equation forms the arc of a circle with its centre below the ε' axis (the so-called Cole–Cole plot) [15].

The relaxation times determined from analysis of the spectra are presented in Figure 7b in the form of Arrhenius plots. The activation enthalpy of **KS 1** in the N phase is relatively small for this type of compound (see, for example, [10, 11]). In compounds **KS 2**, **KS 4**, **KS 5**, **KS 6**, **KS 7, KS 8, KS 11** and **KS 13** the dielectric relaxation spectra for parallel-oriented nematic samples gave very small increments and could not be analysed. However, for **KS 6** a broad relaxation spectrum was observed in the monotropic rotational phase, Figure 8. Two Debye-type semicircles (Equation (5), with $\alpha = 0$) could be fitted to these spectra. Both processes may be ascribed to two independent rotation motions, the whole molecule rotation around the long axis (process 1) and the middle fluoro-phenyl ring rotation around the *p*-axis (process 2). A similar situation appears to occur in the rotational phases of **KS 12** (see Figure 11, later).

In the case of **KS 9**, which has an octyloxy tail, a weak relaxation process for the parallel oriented sample was observed in both the nematic and smectic C phases (Figure 9(a)). A continuous change in the relaxation time at the phase transition, and similar activation barriers in both phases (Figure 9(b)), suggest that the same type of molecular motion (flip–flop jumps around the short axis) takes place in both phases.

A pronounced relaxation process was observed in the smectic A and B phases of **KS 10**, having $-OCF_3$ as lateral substituent (Figure 10(a)). The amplitudes of the absorption spectra are similar in both phases, in spite of a very large jump in the static permittivity at

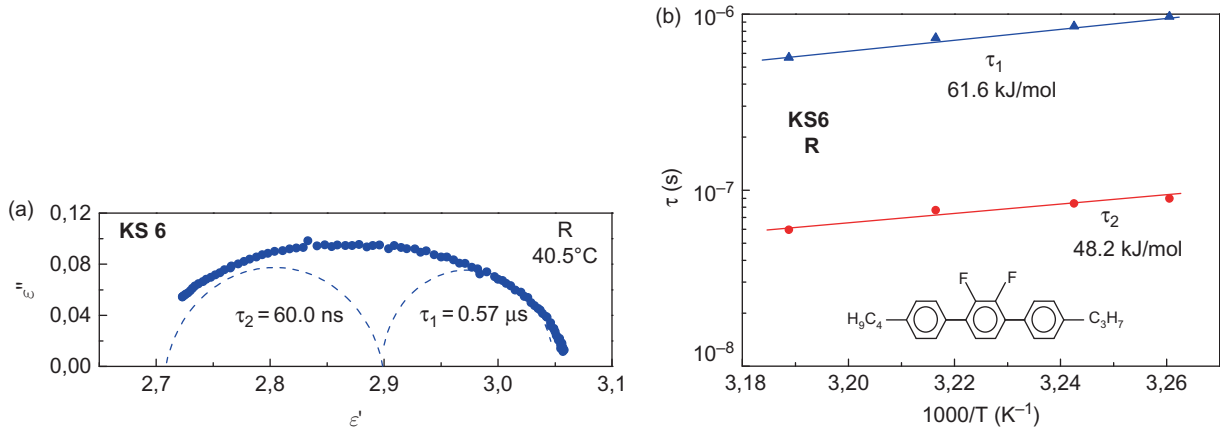

Figure 8. (a) Cole–Cole plot for the spectra collected in the rotator phase of **KS 6**. (b) Arrhenius plot for two relaxation times in the rotational phase with the activation enthalpies indicated (colour version online).

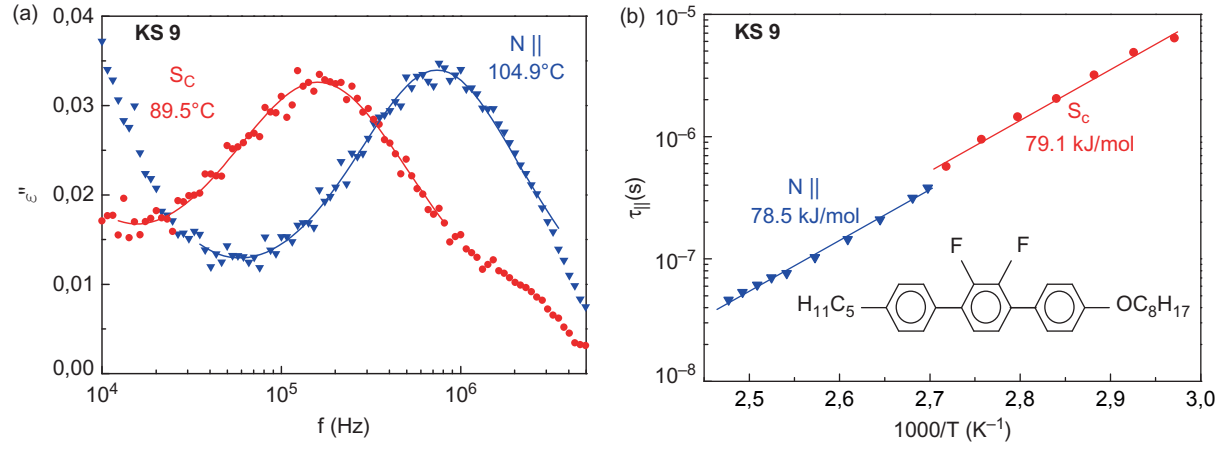

Figure 9. (a) Absorption spectra for the nematic and smectic C phases of **KS 9**; the lines are fits of the Debye-type process with the addition of the conductivity component. (b) Arrhenius plots for the longitudinal relaxation times for both phases (colour version online).

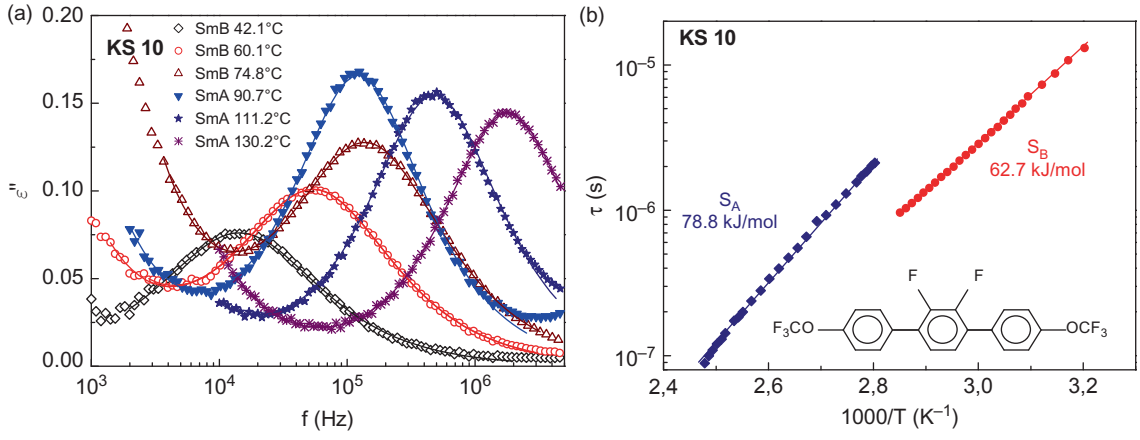

Figure 10. (a) Absorption spectra measured for the SmA and SmB phases of **KS 10**; lines are the fits of the Debye-type formula with the conductivity part. (b) Arrhenius plots for relaxation times for both phases (colour version online).

the SmA–SmB phase transition (see Figure 4(a)). Additionally, the relaxation time becomes shorter after the transition from the liquid-like SmA to the solid-like SmB phase, with a decrease in the activation barrier for the molecular rotation (Figure 10(b)). These observations seem to indicate that the relaxation processes observed are connected with the flip–flop motion in the SmA phase, and with the spinning motion in the SmB phase.

The compounds belonging to the fourth group (**KS 12**–**KS 15**) have an asymmetric dipolar structure in the terphenyl core, so the relaxation process connected with the molecular rotations around the short axes in LC phases should in principle be visible in the kilo- and/or mega-Hertz frequencies. This is what actually happens in **KS 12** and **KS 14**. In the case of **KS 13** and **KS 15** the relaxation process in the parallel-oriented nematic sample was shifted towards low frequencies (below 10 kHz), where the conductivity effect dominates the spectra and the relaxation time could not be determined.

Figure 11(a) gives examples of the spectra collected in the parallel-oriented nematic and the smectic C (SmC) phases of **KS 12**. The Cole–Cole equation, with a small α parameter, describes the spectra very well. The relaxation time smoothly passes through the phase transition, but the activation barrier changes considerably (Figure 11(c)). This process is clearly connected with the molecular rotation around the short axis. Unexpectedly, on cooling the SmC phase, **KS 12** transformed into a solid-like phase in which the relaxation spectra became distinctly stronger (Figure 11(b)). After a further decrease in temperature, a solid-solid phase transition was detected, which is seen as a small but significant jump in the permittivity (see Figure 5(a)). The shapes of the absorption spectra did not, however, change during the transition; they are relatively broad, suggesting the existence of two overlapping relaxation processes in both rotational phases (Figure 11(b)). These processes can be ascribed to the overall and internal rotation motions, similar to the rotational phase of **KS 6** discussed above.

For **KS 14**, a clear relaxation process of the Debye-type was observed in the parallel oriented nematic phase (Figure 12(a)). This corresponds to the molecular rotations around the short axes (large activation enthalpy, Figure 12(c)). A pronounced relaxation process, observed in the monotropic rotational phase (see Figure 5(a)), had a skewed arc form in the Cole–Cole presentation (Figure 12(b)). A superimposition of two processes was assumed in the analysis of the spectra ($k = 2$ in Equation (5)). The relaxation times determined in this manner are presented in Figure 12(c) (the parameter α for the first and second processes is 0.10 and 0.03, respectively). A large dielectric increment for the low frequency process, in which a large dipole moment is involved, indicates that it is connected with the rotation of the whole molecule around the long axis. The unusually large activation barrier determined for this process (~75 kJ mol^{-1}) may be the result of strong dipole–dipole correlations, as discussed earlier. The second relaxation process, with a similar value for the activation barrier, seems to be connected with the intramolecular rotation of the central fluoro-phenyl ring around the *p*-axis.

4. Conclusions

The chemical structures of all the fluoro-substituted terphenyl molecules listed in Table 1 show that in most cases the perpendicular component of the dipole moment should dominate the dielectric properties of the compounds. In fact, the nematic phase exhibits a negative dielectric anisotropy, $\Delta\varepsilon = \varepsilon_{\parallel} - \varepsilon_{\perp} < 0$, whose

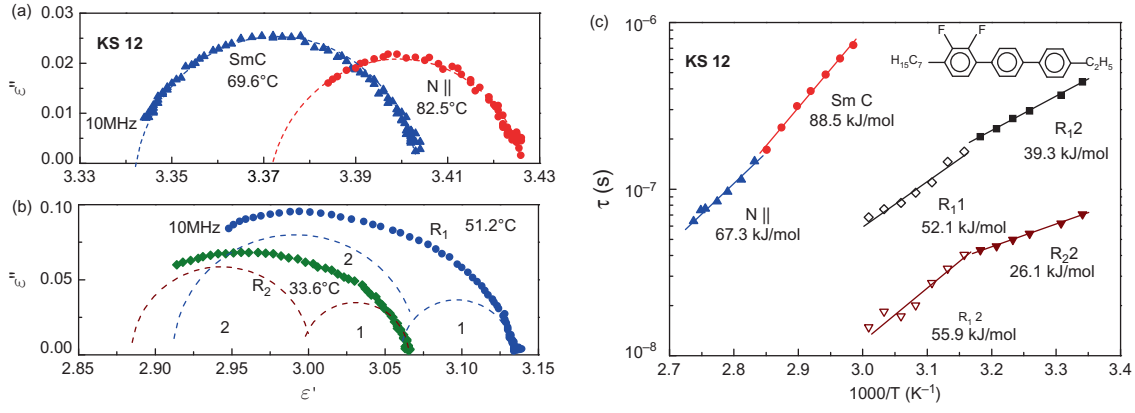

Figure 11. Cole–Cole plots for **KS 12**: (a) in the parallel oriented nematic and in the smectic C phases; the distribution parameter α is about 0.03 in both phases, and (b) in two rotational phases appeared on cooling; two Debye-type semicircles were fitted to the spectra. (c) Activation plots, showing activation enthalpies for all four phases (colour version online).

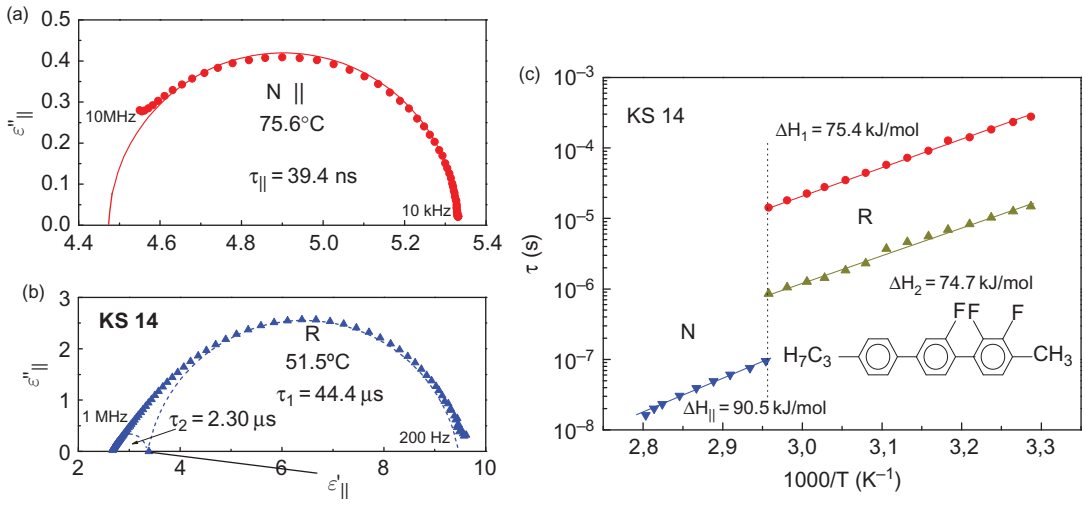

Figure 12. Cole–Cole plots for (a) the nematic and (b) the rotational phases of **KS 14**, and the corresponding activation plots (c) (colour version online).

value depends only slightly on the terminal substituents, but is mainly determined by the number of fluorine atoms attached in the lateral positions. Small or very small values of the longitudinal dipole components cause the relaxation process connected with the molecular rotation around the short axes to produce a negligible dielectric increment. In the case of only five compounds with liquid-like LC phases could the relaxation time and the activation barrier characterising this motion be determined. Very interesting dynamic properties of molecules in the monotropic solid rotator phases have been established. The overall molecular motion around the long axes is accompanied by the intramolecular rotation of the fluoro-phenyl rings around the *p*-axes.

This work has demonstrated that the design of new fluorinated LCs with the desired properties can be supported and projected by adopting a combined spectroscopic and computational approach, and is able to demonstrate an important correlation between experimental observation and molecular properties.

Acknowledgements

This work was partially supported by the executive programme of scientific and technological co-operation between the Italian Republic and Poland 2007–2009 (Project No. 8), and was financed in part by the EU under contract number IST–028154 and by Polish grant PBS 765. Joanna Czub is thanked for her help in carrying out the measurements.

References

[1] Ohmura, K.; Kataoka, S.; Sasaki, T.; Koike, Y. *SID '97 Digest* **1997**, 845–848.

[2] Reiffenrath, V.; Krause, J.; Plach, H.J.; Weber, G. *Liq. Cryst.* **1989**, *5*, 159.

[3] Kirsch, P.; Bremer, M. *Angew. Chem. Int. Ed.* **2000**, *39*, 4216–4235.

[4] Pauluth, D.; Tarumi, K. *Journal of the SID*. **2005**, *13/8*, 693–701.

[5] Kula, P.; Spadło, A.; Dziaduszek, J.; Filipowicz, M.; Dąbrowski, R.; Czub, J.; Urban, S. *Opto-Electron. Rev.* **2009**, *16*, 379.

[6] Frisch, M.J.; Trucks, G.W.; Schlegel, H.B.; Scuseria, G.E.; Rob, M.A.; Cheeseman, J.R.; Montgomery, Jr. J.A.; Vreven, T.; Kudin, K.N.; Burant, J.C.; Millam, J.M.; Iyengar, S.S.; Tomasi, J.; Barone, V.; Mennucci, B.; Cossi, M.; Scalmani, G.; Rega, N.; Petersson, G.A.; Nakatsuji, H.; Hada, M.; Ehara, M.; Toyota, K.; Fukuda, R.; Hasegawa, J.; Ishida, M.; Nakajima, T.; Honda, Y.; Kitao, O.; Nakai, H.; Klene, M.; Li, X.; Knox, J.E.; Hratchian, H.P.; Cross, J.B.; Bakken, V.; Adamo, C.; Jaramillo, J.; Gomperts, R.; Stratmann, R.E.; Yazyev, O.; Austin, A.J.; Cammi, R.; Pomelli, C.; Ochterski, J.W.; Ayala, P.Y.; Morokuma, K.; Voth, G.A.; Salvador, P.; Dannenberg, J.J.; Zakrzewski, V.G.; Dapprich, S.; Daniels, A.D.; Strain, M.C.; Farkas, O.; Malick, D.K.; Rabuck, A.D.; Raghavachari, K.; Foresman, J.B.; Ortiz, J.V.; Cui, Q.; Baboul, A.G.; Clifford, S.; Cioslowski, J.; Stefanov, B.B.; Liu, G.; Liashenko, A.; Piskorz, P.; Komaromi, I.; Martin, R.L.; Fox, D.J.; Keith, T.; Al-Laham, M.A.; Peng, C.Y.; Nanayakkara, A.; Challacombe, M.; Gill, P.M.W.; Johnson, B.; Chen, W.; Wong, M.W.; Gonzalez, C.; Pople, J.A. *Gaussian 03, revision E.05*; Pittsburgh, PA: Gaussian, Inc., 2003.

[7] Becke, A.D. *Phys. Rev. A: At., Mol., Opt. Phys.* **1988**, *38*, 3098.

[8] Lee, C.; Yang, W.; Parr, R.G. *Phys. Rev. B* **1988**, *37*, 785.

[9] Minkin, W.I.; Osipov, O.A.; Zhdanov, U.A. *Dipole Moments in Organic Chemistry*; New York: Plenum Press, 1970.

[10] Czub, J.; Urban, S.; Dabrowski, R.; Gestblom, B. *Acta Phys. Pol., A* **2005**, *107*, 947.

[11] Czub, J.; Dabrowski, R.; Dziaduszek, J.; Urban, S. *Phase Transitions* **2009**, *82*, 485.
[12] Jadżyn, J.; Legrand, C.; Czechowski, G.; Bauman, D. *Liq. Cryst.* **1998**, *24*, 689.
[13] Douali, R.; Czechowski, G.; Legrand, C.; Jadżyn, J. *Acta Phys. Pol.* **2004**, *105A*, 365.
[14] Calucci, L.; Geppi, M. *J. Chem. Inf. Comput. Sci.* **2001**, *41*, 1006.
[15] Chelkowski, A. *Dielectric Physics*; Amsterdam: Elsevier, 1980.
[16] Maier, W.; Meier, G. *Z. Naturforsch*. **1961**, *16a*, 470.
[17] Catalano, D.; Geppi, M.; Marini, A.; Veracini, C.A.; Urban, S.; Czub, J.; Kuczyński, W.; Dąbrowski, R. *J. Phys. Chem. C* **2007**, *111*, 5286.
[18] Geppi, M.; Marini, A.; Veracini, C.A.; Urban, S.; Czub, J.; Kuczyński, W.; Dąbrowski, R. *J. Phys. Chem. B* **2008**, *112*, 9663.
[19] Borsacchi, S.; Calucci, L.; Czub, J.; Dąbrowski, R.; Geppi, M.; Kuczyński, W.; Marini, A.; Mennucci, B.; Urban, S. *J. Phys. Chem. B* **2009**, *113*, 15783.